**The EMBO Journal (2009) 28,** 745–754 | © 2009 European Molecular Biology Organization | All Rights Reserved 0261-4189/09
www.embojournal.org

THE EMBO JOURNAL

# Structural basis for competitive interactions of Pex14 with the import receptors Pex5 and Pex19

**Christian Neufeld[1,2], Fabian V Filipp[1,6], Bernd Simon[1], Alexander Neuhaus[3], Nicole Schüller[2], Christine David[3], Hamed Kooshapur[4,5], Tobias Madl[4,5], Ralf Erdmann[3], Wolfgang Schliebs[3], Matthias Wilmanns[2] and Michael Sattler[1,4,5,*]**

[1]EMBL Heidelberg, Heidelberg, Germany, [2]EMBL Hamburg Outstation, c/o DESY, Hamburg, Germany, [3]Institute for Physiological Chemistry, Department of Systems Biology, Faculty of Medicine, Ruhr University of Bochum, Bochum, Germany, [4]Helmholtz Zentrum München, Neuherberg, Germany and [5]Munich Center for Integrated Protein Science and Biomolecular NMR, Department Chemie, Technische Universität München, Garching, Germany

**Protein import into peroxisomes depends on a complex and dynamic network of protein–protein interactions. Pex14 is a central component of the peroxisomal import machinery and binds the soluble receptors Pex5 and Pex19, which have important function in the assembly of peroxisome matrix and membrane, respectively. We show that the N-terminal domain of Pex14, Pex14(N), adopts a three-helical fold. Pex5 and Pex19 ligand helices bind competitively to the same surface in Pex14(N) albeit with opposite directionality. The molecular recognition involves conserved aromatic side chains in the Pex5 WxxxF/Y motif and a newly identified F/YFxxxF sequence in Pex19. The Pex14–Pex5 complex structure reveals molecular details for a critical interaction in docking Pex5 to the peroxisomal membrane. We show that mutations of Pex14 residues located in the Pex5/Pex19 binding region disrupt Pex5 and/or Pex19 binding *in vitro*. The corresponding full-length Pex14 variants are impaired in peroxisomal membrane localisation *in vivo*, showing that the molecular interactions mediated by the N-terminal domain modulate peroxisomal targeting of Pex14.**

*The EMBO Journal* (2009) **28,** 745–754. doi:10.1038/emboj.2009.7; Published online 5 February 2009
*Subject Categories*: structural biology
*Keywords*: import receptor; NMR; peroxisome biogenesis; peroxisomes; structural biology

## Introduction

Peroxisomes are ubiquitous, single membrane cell organelles with a large variety of metabolic functions. Most, if not all proteins participating in peroxisomal biogenesis, collectively called peroxins or Pex proteins have been identified (Erdmann and Schliebs, 2005). Mutations in Pex proteins are implicated in diseases, such as the spectrum of Zellweger disorders (Wanders and Waterham, 2006). However, molecular details of the functional activity of peroxins and their involvement in these diseases are poorly understood.

The membrane-associated protein Pex14 has been described as a central component of the translocation machinery for peroxisomal matrix enzymes. Because of its direct interaction with the peroxisome targeting signal (PTS) receptor Pex5, Pex14 has been proposed to serve as the docking site for the cytosolic receptor–cargo complex (Albertini *et al*, 1997). Pex14 sequences from different organisms display a common domain composition, consisting of a conserved N-terminal domain, a segment of hydrophobic amino acids and a coiled-coil region (Albertini *et al*, 1997; Shimizu *et al*, 1999; Will *et al*, 1999; Shimozawa *et al*, 2004). Mammalian Pex14 is an integral membrane protein, with its C-terminus exposed to the cytosol and a potential for homo-oligomerisation (Will *et al*, 1999; Otera *et al*, 2002; Itoh and Fujiki, 2006). The recognition of one or multiple aromatic WxxxF/Y motifs in Pex5 by the N-terminal Pex14 domain have an important function for docking of the Pex5 receptor to the peroxisomal membrane (Saidowsky *et al*, 2001; Otera *et al*, 2002; Choe *et al*, 2003; Williams *et al*, 2005).

Pex19, a mainly cytosolic peroxin, has been proposed to serve as a translocation receptor and chaperone of newly synthesised peroxisomal membrane proteins (PMP) (Sacksteder *et al*, 2000). It recognises a composite peroxisomal membrane protein targeting signal (mPTS), which may involve different regions of the PMP proteins and—in contrast to PTSs PTS1/PTS2—cannot be represented by a simple consensus sequence (Rottensteiner *et al*, 2004; Halbach *et al*, 2005, 2006; Saveria *et al*, 2007). In contrast, binding of Pex19 to the PMP Pex14 depends on a small central region in Pex19 and a conserved N-terminal domain in Pex14 (Fransen *et al*, 2002), which does not contain an identifiable mPTS motif. Because both Pex5 and Pex19 bind to the same region in Pex14, it has been suggested that Pex19 might have a function in the peroxisomal matrix protein import (Fransen *et al*, 2004).

Here, we present the molecular basis for the interaction of the N-terminal domain of Pex14, Pex14(N), with Pex5 and Pex19. We identified an F/YFxxxF motif in the N-terminus of Pex19, which binds to the same site in Pex14 as the Pex5 WxxxF/Y motif. The three-dimensional solution structures of Pex14(N)-ligand complexes provide molecular details for the recognition of conserved aromatic residues in the Pex5 and Pex19 ligand motifs and show that the two peptides bind to Pex14 with opposite directionality. Competitive NMR titration experiments and quantification of both interactions by isothermal titration calorimetry reveal that Pex5 binds with significantly higher affinity. The Pex14–Pex5 complex

*Corresponding author. Institute of Structural Biology, Helmholtz Zentrum Muenchen, Ingolstaedter Landstr. 1, Neuherberg, 85764, Germany. Tel.: +49 89 28913418; Fax: +49 89 28913869; E-mail: sattler@helmholtz-muenchen.de
[6]Present address: Department of Chemistry and Biochemistry, University of California, San Diego, La Jolla, CA 92093-0307, USA

**Received: 21 May 2008; accepted: 5 January 2009; published online: 5 February 2009**

provides a structural basis for the docking of Pex5 to Pex14 at the peroxisomal membrane. Pex14(N) variants, which impair binding to Pex5 and/or Pex19 *in vitro*, exhibit a subcellular mislocalisation *in vivo*, suggesting that the binding interface contributes to the targeting of Pex14 to the peroxisomal membrane.

## Results

### *Competitive binding of Pex5 and Pex19 peptides to Pex14*

The N-terminal region of Pex14(N), comprising residues 16–80, was found to be resistant against exopeptidases (data not shown) and selected to study the interactions with peptide ligands derived from Pex5 and Pex19. For Pex5, three peptides of different length (residues 116–124, 113–127 and 108–127) where chosen. These peptides all comprise the first WxxxF/Y motif, representing the strongest Pex14 interaction site (Saidowsky *et al*, 2001). For Pex19, a peptide comprising residues 66–77 was selected (Figure 1A). It contains the sequence segment (67–72) that was shown to be critical for Pex14 binding (Fransen *et al*, 2005).

The binding of the Pex19 and Pex5 ligands to Pex14(N) was first studied by NMR titration experiments. Unlabelled Pex5(116–124) or Pex19(66–77) peptides were titrated to saturation into a solution of $^{15}$N-labelled Pex14(16–80). Changes of amide chemical shifts were monitored in two-dimensional $^{1}$H, $^{15}$N-HSQC experiments (Figure 1B). Chemical shift assignments of Pex14(N) were obtained using standard methods (Sattler *et al*, 1999). Mapping of residues that experience significant chemical shift perturbations onto the primary sequence of Pex14 revealed that both peptides bind to an overlapping site involving helices α1 and α2 and the connecting linker (Figure 1C). The binding of Pex19 to Pex14(N) is fast on the NMR chemical shift timescale, as judged from the gradual change of the NMR signals in the HSQC spectra on addition of increasing amounts of ligand. In contrast, the appearance of new signals corresponding to the bound state during the titration of Pex14(N) with the Pex5 peptide shows binding in the slow exchange limit, indicative of a tighter interaction with the Pex5 ligand (Figure 1B).

To confirm that the binding sites are overlapping, a double-titration experiment was performed, where the Pex19 peptide was added to saturation to $^{15}$N-labelled Pex14(N) followed by a cross-titration with the Pex5 ligand (Figure 1D). The chemical shifts observed at the endpoint of the cross-titration (molar ratios of 1:1.5:1.5 Pex14(N):Pex19:Pex5) are identical to those seen on addition of the Pex5 peptide alone. This shows that the Pex19 ligand is replaced by the stronger interaction of the Pex5 peptide with Pex14.

The binding affinities of the peptides, as determined by isothermal titration calorimetry, reveal equilibrium dissociation constants ($K_D$) of 0.47 μM for Pex5(116–124)–Pex14(N) interaction and 9 μM for Pex19–Pex14(N) interaction. Longer Pex5 peptides bind to Pex14(N) with higher affinities, that is, $K_D$ of 0.12 μM for Pex5(113–127) and 0.07 μM for Pex5(108–127) (Supplementary Table 1). This suggests that the residues flanking the aromatic core motif of Pex5 further contribute to the interaction. However, irrespective of the length of the Pex5 peptide, the binding affinity is considerably higher than that measured for the Pex19 peptide, thus supporting our data from Pex5/Pex19 binding competition experiments on Pex14(N).

### *Three-dimensional structures of Pex14(N) bound to Pex5 and Pex19 peptides*

The three-dimensional structures of the N-terminal domain of Pex14 in complex with peptides derived from Pex5 (residues 108–127) and Pex19 (residues 66–77) were determined using heteronuclear NMR methods (Supplementary Table 2). The core region of Pex14(N) (residues 23–73) adopts a well-defined conformation, whereas N- and C-terminal flanking residues are flexible and do not display a defined secondary structure (Supplementary Figures 1 and 2). The structures of the Pex14–Pex5 and Pex14–Pex19 complexes are well defined by the NMR data, which include 130/112 intermolecular NOEs for the Pex5 and Pex19 complexes, respectively (Supplementary Table 2; Figure 2).

Pex14(N) comprises three α-helices, forming a three-helical bundle. Helices α1 and α2 are in an anti-parallel orientation (Figure 2), whereas helix α3 forms a scaffold diagonal across the pair of helices α1 and α2. A short helical turn is found in the linker connecting helix α1 and α2. Secondary chemical shifts of free Pex14(N) indicate that the secondary structure of the ligand-free Pex14(N) domain is very similar to the Pex5 or Pex19 bound form, with the exception of the helical turn in the α1–α2 linker, which is induced on ligand binding (Supplementary Figure 2).

Overall, the Pex14(N) conformation in the Pex14(N)/Pex5 and Pex14(N)/Pex19 complexes is very similar, reflected by a low coordinate r.m.s.d of 1.1 Å when superimposing the Pex14(N) backbone. The size of the protein–peptide binding interface is $\approx$460 Å$^2$ in both complexes. Comparison of the secondary chemical shifts of the free and Pex14(N) bound ligand peptides indicates that a helical conformation of the Pex5 peptide is present irrespective of Pex14(N) binding, whereas for the free Pex19 peptide, only a small fraction of helical conformation has been detected (data not shown).

The binding site of Pex14(N) with Pex5 and Pex19 is formed by helices α1 and α2 (Figure 3A–C) and exhibits two hydrophobic pockets, which are separated by two aromatic residues (Phe35 and Phe52) (Figures 3, 4A and B). The two hydrophobic pockets are flanked by several basic amino acids (Arg25, Lys34, Arg40, Lys55 and Lys56), leading to a highly positively charged protein surface (Figure 3A). In contrast, the binding surfaces of the Pex5 and Pex19 ligands contain negatively charged surface patches (Figure 3D), suggesting that charge complementarity is a key determinant of the observed Pex14(N)–Pex5 and Pex14(N)–Pex19 interactions. The electrostatic surface representation of both complexes exhibits a three-layered arrangement, where the two positively charged helices α1 and α2 in Pex14(N) are flanked by the negatively charged helix α3 on one side and by the negatively charged Pex5 and Pex19 ligands on the other side (Figure 3C).

In the Pex14(N)–Pex5 complex, the Pex5 peptide adopts an amphipathic α-helical conformation and binds diagonally across helices α1 and α2 in Pex14(N) (Figures 2B and 4A). The conserved aromatic residues in the Pex5 WxxxF/Y motif, Trp118 and Phe122, are deeply buried into the two separate hydrophobic pockets in Pex14(N) (Figure 4A). The aromatic side chain of Pex5 Trp118 is stabilised by stacking on one side with the side chain of the highly conserved Pex14 Lys56 and

 

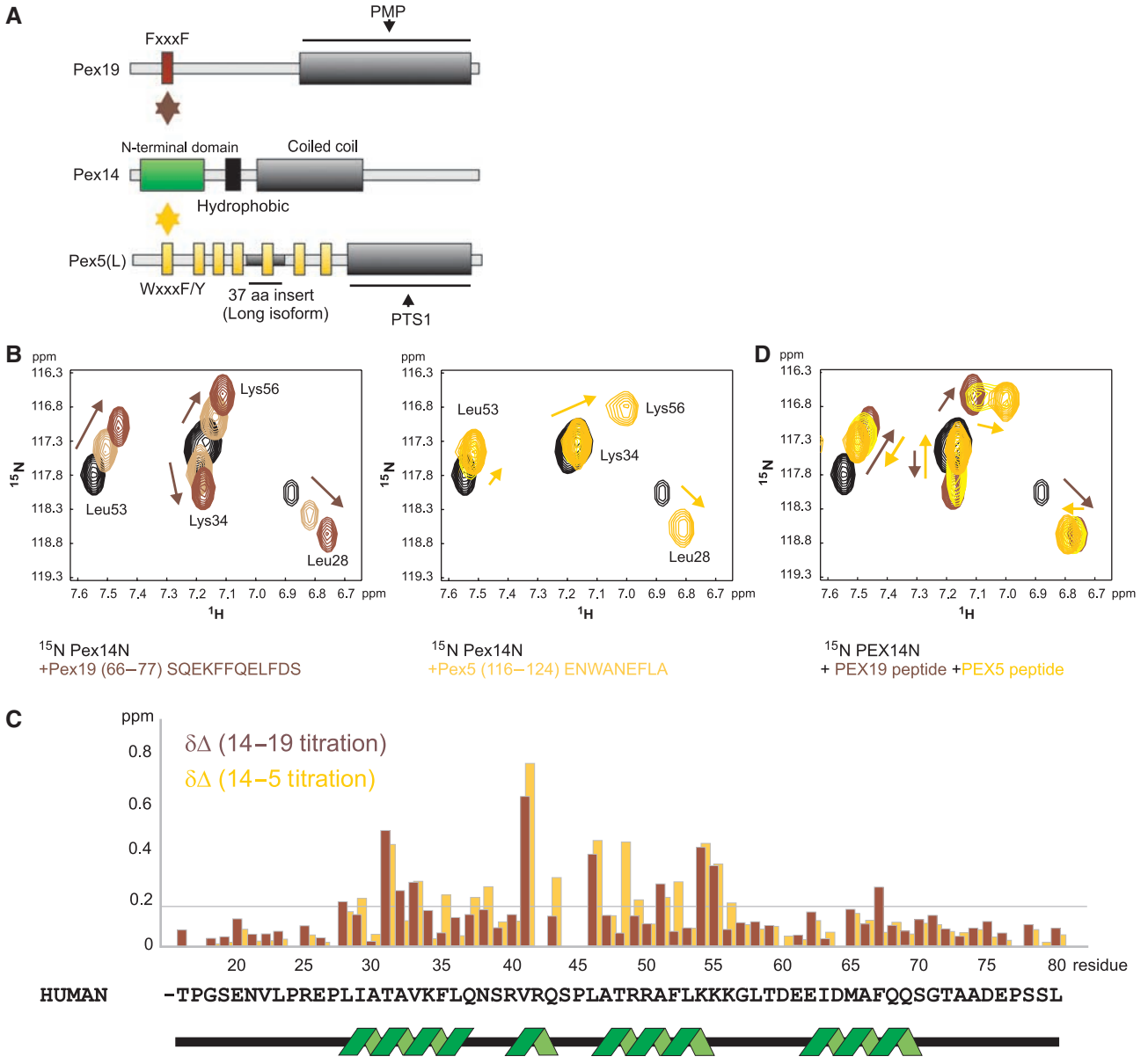


**Figure 1** NMR titrations of Pex14(N) with Pex19 and Pex5 peptides. (**A**) Schematic overview of the domain composition of human Pex5, Pex19 and Pex14. The N-terminal domain of Pex14 is coloured green, the binding motifs are shown in brown (Pex19) and gold (Pex5), respectively. (**B**) $^{1}H$,$^{15}N$ correlation spectra of $^{15}N$-labelled recombinant Pex14(N) free (black), and in complex with Pex19 (residues 66–77) (brown; left) and Pex5 (gold; right) (residues 116–124). (**C**) NMR chemical shift changes ($\Delta\delta = (\delta^2_{15N} + \delta^2_{1H})^{1/2}$) of Pex14(N) in the presence of saturated concentrations of the Pex5 (gold) and the Pex19 (brown) ligands. Secondary structure elements are indicated underneath. (**D**) $^{15}N$-labelled recombinant Pex14(N) (black) was titrated with Pex19(66–77) (brown) to the point of saturation and was then cross-titrated with Pex5(116–124) (gold).

on the other side with the methyl group of Pex14 Thr31. In addition, the NMR ensemble indicates a salt bridge between Pex5 Glu121 and the Pex14 Lys56 side chain. Pex5 Phe122 mainly interacts with two aromatic residues (Phe35 and Phe52) in Pex14 that separate the two binding pockets.

In the Pex14(N)–Pex19 complex structure, the Pex19 peptide also forms an amphipathic helix that binds across α1 and α2 helices of Pex14, similar to the Pex5–Pex14 complex (Figures 2D and 4B). However, in contrast to the Pex14(N)–Pex5 complex, the Pex19 helix binds in an almost opposite orientation (Figure 2; Supplementary Figures 3 and 4). Because of the inverted orientation, Phe75 at the C-terminal side of the Pex19 F/YFxxxF motif occupies the binding pocket used by Pex5 Trp118 in the Pex14(N)–Pex5 complex. The Pex19 Phe75 side chain is stabilised by similar interactions as seen for Pex5 Trp118. In contrast, the second hydrophobic-binding pocket in Pex14(N) is distinct in the Pex5 and Pex19 complexes. Pex19 Phe71 interacts with Pex14 Phe35, Thr48 and Phe52, resembling the recognition of the corresponding Phe122 in Pex5. However, it is less deeply inserted into the binding pocket (Figures 3A and 4). The preceding Pex19 Phe70 residue contacts Pex14(N) in a neighboring region. In contrast to the corresponding L123 in the Pex5 complex, the aromatic side chain of Pex19 Phe70 is stabilised by a stacking interaction with the guanidinium group of Pex14 Arg 40 (Figure 4A and B).

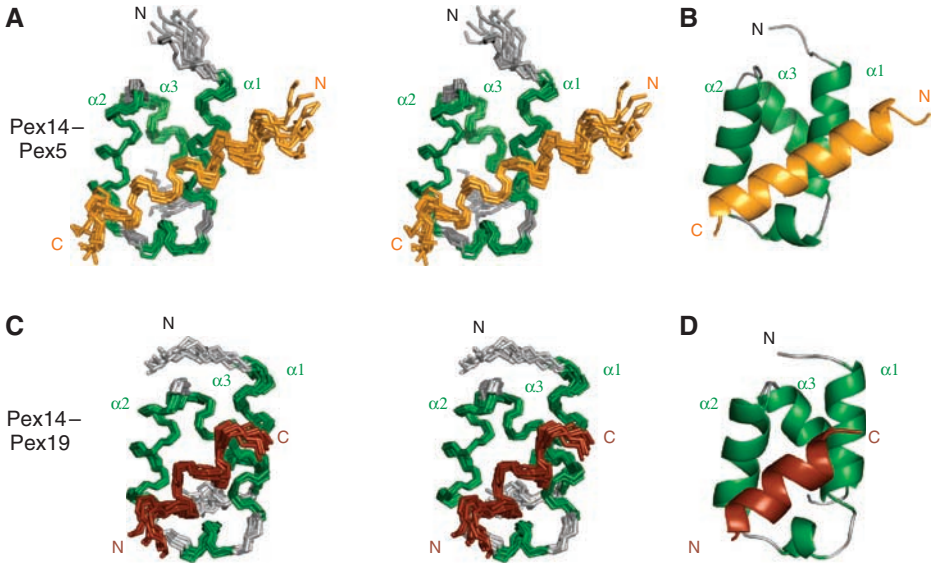


**Figure 2** Solution structures of the Pex14(N)–Pex5 and Pex14(N)–Pex19 complexes. (**A**) Stereo view of the backbone atoms of Pex14 (residues 20–76) in complex with Pex5(108–127). An NMR ensemble of the 10 lowest-energy structures (out of 100 calculated) is shown. Secondary structure elements in Pex14 (helices α1, α2, α3 and the helical linker connecting α1 and α2) are coloured in green. The peptide is shown in gold. (**B**) Ribbon diagram of the lowest-energy structure in (A). (**C**) Superposition of the backbone atoms of Pex14 (residues 19–76) in complex with Pex19(66–77). The ensemble shows 10 lowest-energy structures (out of 100 calculated). The peptide is shown in brown. (**D**) Ribbon presentation of the lowest-energy structure in (C).

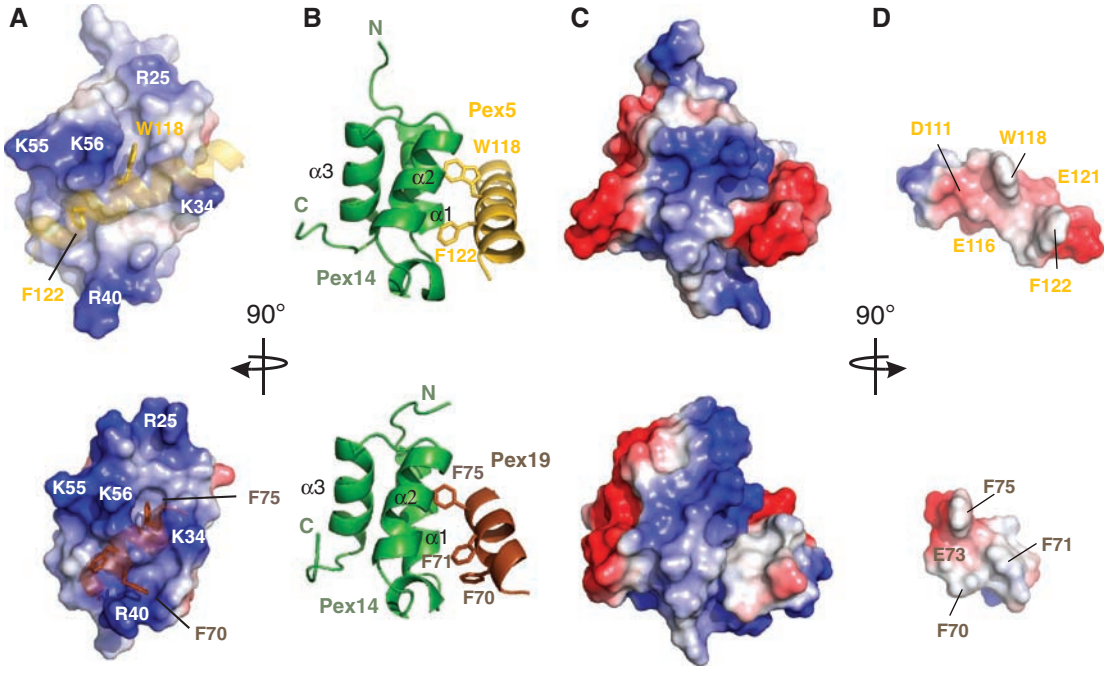


**Figure 3** Electrostatic surface representation of the Pex14–Pex5 and Pex14–Pex19 complexes. The Pex14(N)–Pex5 and Pex14(N)–Pex19 complex structures are shown in the top and bottom rows, respectively. (**A**) View onto the ligand-binding surface. The Pex5 and Pex19 ligand helices are shown as transparent ribbons. Blue and red colours indicate positive and negative electrostatic surface potential in Pex14. Positively charged residues in Pex14(N) surrounding the binding interface are labelled. (**B**) Ribbon representation of the Pex14(N)–Pex5 (top) and Pex14(N)–Pex19 complexes. The aromatic residues in the two ligands are shown and labelled. Pex14(N), Pex5 and Pex19 are coloured in green, gold and brown, respectively. (**C**) Surface representation of the two complexes shown in the same orientation as in (B). Blue and red colours indicate positive and negative electrostatic surface potential, respectively. (**D**) Surface representation of the Pex5 (top) and Pex19 (bottom) ligands bound to Pex14, as viewed from the Pex14 interaction surface.

The orientation of the helical axes of the Pex19 and Pex5 ligands differs by 17° (Supplementary Figure 3). An exact opposite orientation would not allow efficient interactions of all three-aromatic residues in the Pex19 F/YFxxxF motif to both hydrophobic-binding pockets in Pex14 (not shown). To independently confirm the observed opposite orientation of the Pex19 peptide, we performed paramagnetic relaxation enhancement experiments, with a Pex19(S66C) mutant

 

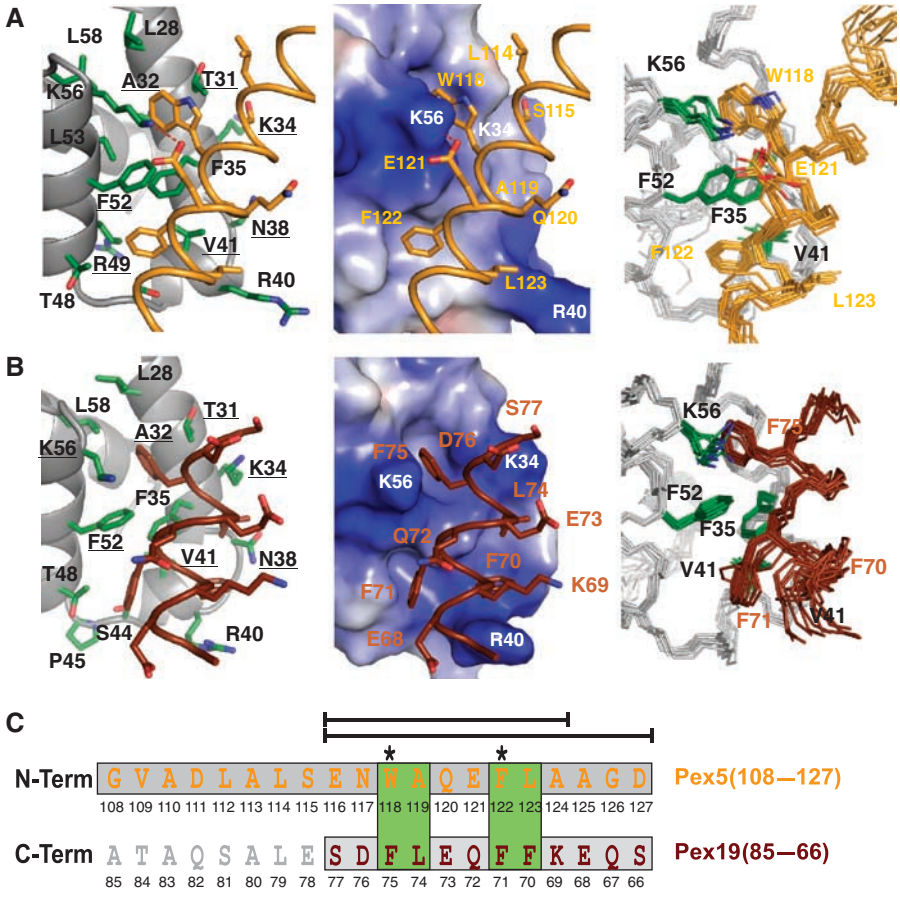


**Figure 4** Structural details of the Pex14–Pex5 and Pex14–Pex19 interactions. Ribbon (left), surface (middle) and ensemble (right) representations of the molecular interface between Pex14 and Pex5(108–127) (**A**) and Pex19(66–77) (**B**). Left: Pex14 is shown in grey, the Pex5 and Pex19 peptides are coloured gold and brown, respectively. Residues showing intermolecular NOEs are shown in stick representation. Pex14 side chains are coloured in green, peptide backbone and side chains are in gold (Pex5) or brown (Pex19). Positively charged Pex14(N) residues are labelled white. An intermolecular salt bridge between Pex14(N) Lys56 and Pex5 Glu121 is indicated by a dashed red line. Labelling of Pex14 residues that were altered for mutational analysis are underlined. (**C**) Sequences of Pex5 and Pex19 peptide ligands used for binding and structural studies. The peptide fragments used for structure determination are shown with grey background. The Pex5 and Pex19 sequences are aligned based on the structural analysis and are shown with opposite directionality. Smaller Pex5 peptides are indicated by the lines above the sequence (see Supplementary Table 1). Pex5 Glu121, which forms an electrostatic contact with Pex14 Lys56, is highlighted in red. Conserved hydrophobic residues are highlighted in green, the two critical aromatic residues in both peptide motifs are marked with an asterisk.

peptide that allows the covalent attachment of a paramagnetic proxyl group. Binding of the spin-labelled Pex19 variant to Pex14(N) leads to line broadening of the amide proton signals of Pex14(N) residues 40–56 (Supplementary Figure 4C). As spin-label effects strongly decrease with distance, and the relaxation enhancements induced are sensitive in detecting even small populations of conformations with close proximity to the spin label, a Pex5-like orientation of the Pex19 peptide can be excluded.

### *Specificity of the Pex5 and Pex19 interactions analysed by peptide scan*

To investigate the structural requirements for the binding of Pex5 and Pex19 peptides by independent means, we identified critical residues in the respective interaction motifs by systematic mutational analysis. Pex14(N) was purified as a recombinant polyhistidine fusion protein and incubated with a cellulose membrane containing a set of peptide sequences in which each residue in the core binding motifs of Pex5(113–127) or Pex19(66–80) was substituted by all other 19 amino acids. Binding of Pex14(N) was detected by monoclonal anti-polyhistidine-tag antibodies (Figure 5).

A common observation for both peptides is that Pex14(N) does not bind to any ligand containing a proline within the core binding region, consistent with the requirement of an α-helical conformation for Pex14 binding. As expected from our structural analysis, the aromatic residues within the Pex5 sequence are most sensitive for substitutions (Figure 5A). Trp118 and Phe or Tyr at position 122 are strictly required for Pex14(N) binding. Glu121 can be substituted with glutamine and methionine, whereas aspartate at this position, for instance, impairs Pex14(N) binding. Replacement of Leu123 is restricted to other hydrophobic residues. The mutational analysis of the Pex14(N)–Pex19 interaction (Figure 5B) confirms that the binding is mediated mainly by the three-aromatic residues Phe70, Phe71 and Phe75. Interestingly, a version of the Pex19 peptide with an engineered Pex5-like WxxxF/Y motif, Pex19(F75W), does not generate an efficient Pex14(N) binding motif. Modelling of this mutation onto the Pex14(N)–Pex19 complex structure indicates that binding to Pex19 F75W would require a rotation of the ligand helix to

accommodate Trp75, which—in turn—would lead to a steric clash of Pex19 Leu74 and Pex19 Phe70, with the C-terminal part of helix α1 of Pex14(N). Finally, solvent-exposed residues of Pex19 are only exchangeable with negatively charged or neutral residues. A similar preference is also found for the Pex5 interaction (Figure 5A and B). This indicates a requirement of negative charges in the Pex5 and Pex19 ligands for binding to a positively charged surface in Pex14(N) (Figures 3 and 4).

### *Mutational analysis of the Pex14 binding surface*

To validate our findings under physiological conditions, we designed a series of single-residue mutations at the interaction surface of Pex14(N), which are expected to interfere with the binding of Pex19 and/or Pex5. Each mutation was introduced into a full-length Pex14 expression construct for localisation studies in human cells and into an *Escherichia coli* Pex14(N) expression plasmid for *in vitro* binding studies (Figure 6). We selected eight Pex14(N) residues (Thr31, Ala32, Lys34, Asn38, Val41, Arg49, Phe52 and Lys56) that are involved in the formation of the Pex14(N) binding surface for Pex5 and Pex19. We changed the residues into either alanines, leading to removal of specific side-chain contributions, or amino acids that are expected to introduce either steric clashes (A32W, F52W) or repulsive, charged interactions (R49E, K56E) on complex formation. The tertiary structures of most of these Pex14(N) variants are not affected by the mutations, as judged from the similarity of the NMR spectra of wild-type and mutant proteins (Supplementary Figure 5). However, this is not true for the A32W and R49E mutants, which are less stable and/or aggregate in solution. The Pex14(N) variants were tested at a concentration of 1 μM for their ability to interact with the Pex5(113–127) and Pex19(66–80) peptides (Figure 6A). From the structurally

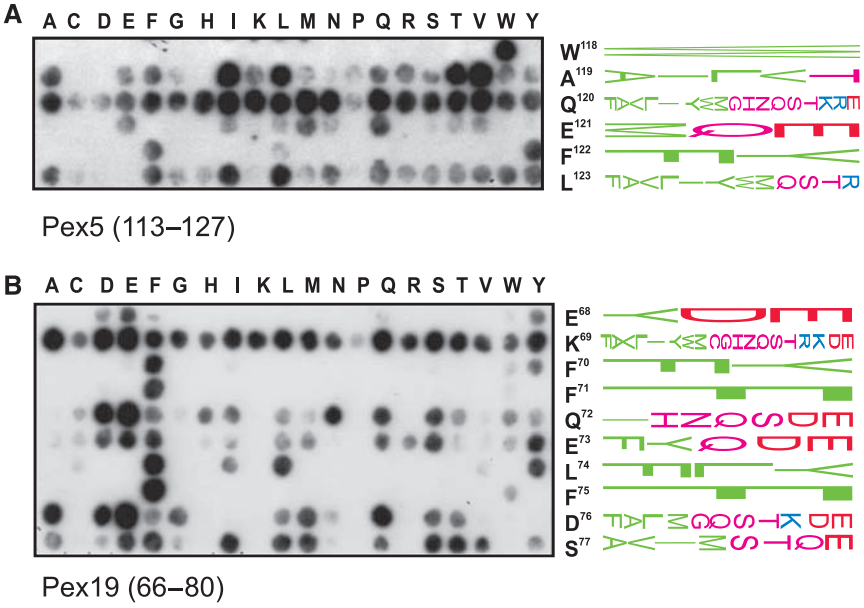


**Figure 5** Mutational analysis of Pex14 and its ligands. N-terminal Pex14 was tested for interactions with variants of Pex5 (**A**) and Pex19 (**B**) peptides. Peptides comprising systematic variations of Pex5 (residues 113–127; ALSENWAQEFLAAGD) and Pex19 (residues 66–80; SQEKFFQELFDSELA) ligands were synthesised on cellulose membranes and incubated with purified $His_6$-Pex14(1–80). Bound Pex14 was visualised immunochemically with monoclonal anti-$His_6$ antibodies. Spots with reduced intensities represent peptides with reduced binding affinities for Pex14. Amino acids that retain the interaction are shown by their single letter code on the right, where the letter size indicates the relative contribution to the interaction at each sequence position. Green and magenta colours indicate hydrophobic or polar/small residues. Red and blue colours display negatively or positively charged residues, respectively.

**Figure 6** *In vitro* and *in vivo* effects of single-site mutations within Pex14(N). (**A**) Left: Pex14 Phe52 and Lys56 are critical for Pex19 binding. His-tagged Pex14(N) variants harbouring the indicated mutations were expressed in *E. coli*, purified, incubated at two different concentrations (1 μM, upper rows; 45 nM, lower row) with immobilised Pex5(113–127) and Pex19(66–80) peptides and detected by anti-Pex14 antibodies. Right: The location of the residues used for the mutational analysis is schematically indicated on the Pex14(N) structure. (**B**, **C**) Full-length Pex14 mutants show various patterns of cellular staining. (B) All single-point mutations lead to partial mitochondrial mislocalisation of full-length Pex14. A Zellweger patient Pex14-deficient fibroblast cell line was transfected with plasmids encoding Pex14 full-length proteins and analysed by immunofluorescence microscopy using antibodies against Pex14 (green, Alexa Fluor 488) and against a mitochondrial marker protein TRAP1 (red, Alexa Fluor 594). Most of the cells expressing Pex14(K56E) and Pex14(F52W), shown as representative examples, display a congruent pattern (yellow colour), showing mitochondrial mislocalisation of Pex14. (C) Pex14 variants can also associate with peroxisomes. Pex14-deficient fibroblasts were co-transfected with plasmids encoding the peroxisomal marker protein GFP-PTS1 and Pex14(K56E) and analysed by fluorescence microscopy (green, EGFP) and immunofluorescence microscopy using antibodies against Pex14 (red, Alexa Fluor 594), respectively. About 10% of the double-transfected cells exhibit a congruent punctuate staining pattern (yellow colour), showing peroxisomal localisation of this Pex14 variant. Bar: 10 μm. (**D**) Quantitative analysis of the mutational effects on the subcellular localisation of Pex14 has been performed for each mutation. Between 75 and 100 double-transfected cells expressing both GFP-PTS1 and one of the Pex14 mutants were inspected for particulate co-localisation of both proteins. Numbers of cells with a peroxisome localisation of Pex14 are given in percent for each mutant.

unaffected variants (thus, not considering A32W and R49E), the mutations F52W, F52A, K56E and, to some extent, K34A decrease the binding affinity to Pex19, whereas at this concentration, the binding to Pex5 is less affected. When the Pex14 proteins were tested at lower concentrations (45 nM), only the F52W mutation did not significantly decrease the Pex5 binding affinity, suggesting that this mutation selectively impairs the Pex19 interaction.

To study the effects of the same mutations *in vivo*, the full-length mutant Pex14 variants were expressed in the Zellweger cell line K-01 T, which is devoid of functional Pex14 (Shimozawa *et al*, 2004). The intracellular localisation

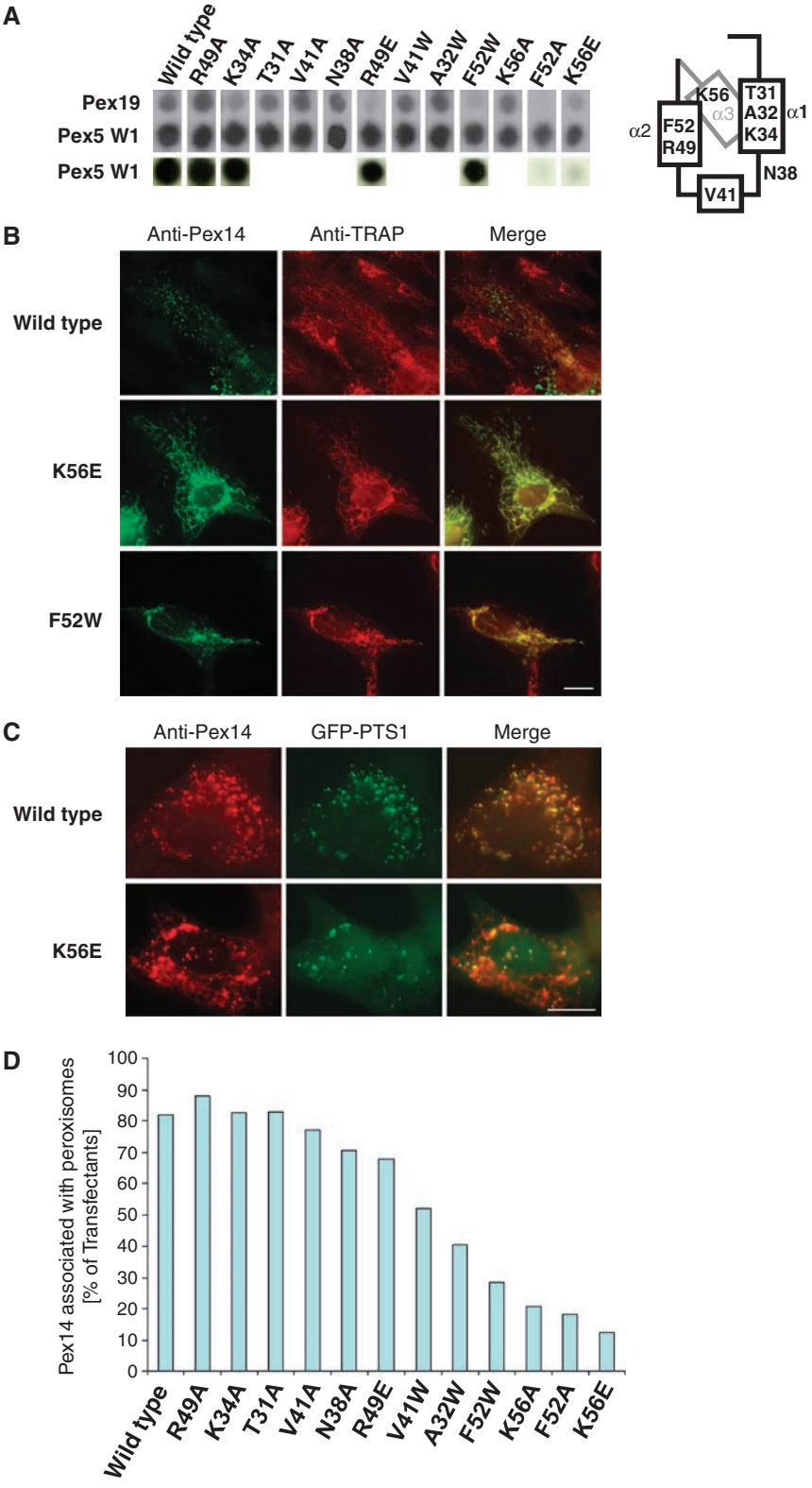

of wild-type and mutant Pex14 was assessed by immunofluorescence microscopy. The subcellular distribution of the different Pex14 mutants showed cell-to-cell variation, as exemplified for Pex14(K56E) (Figure 6B and C). Consistent with previous observations (Itoh and Fujiki, 2006), mutagenesis of the N-terminal domain of mammalian Pex14 can often result in a mitochondrial mislocalisation, as indicated by colocalisation of Pex14(K56E) and Pex14(F52W) with the mitochondrial marker protein TRAP1 (Figure 6B). In contrast, in several cells expressing Pex14(K56E), the congruent punctuate fluorescence pattern of this Pex14 mutant and the peroxisomal marker protein GFP-PTS1 (Figure 6C) or the peroxisomal membrane protein PMP70 (data not shown) indicates peroxisomal localisation. The heterogeneity of the subcellular localisation of Pex14 variants might reflect different expression levels or other factors, such as distinct folding rates. Therefore, for each mutation, an average of approximately 100 cells transfected with both GFP-PTS1 and the different Pex14 mutants was analysed (Figure 6D). For each inspected cell line, at least a few cells exhibited normal peroxisomal import (Figure 6C and D), showing that none of the mutations led to a complete loss-of-function of Pex14. The most severe defects in targeting of Pex14 and the resulting mislocalisation of the peroxisomal GFP-PTS1 are observed in cells expressing Pex14 harbouring mutations of residues Lys56 and Phe52. Notably, these residues are also most critical for Pex19 and Pex5 binding *in vitro* (Figures 4 and 6A).

## Discussion

Here we present the three-dimensional structure of a novel 50-residue fold in the N-terminus of human Pex14. On the basis of the evolutionary conservation of this region (Supplementary Figure 2A), a similar structure is expected for orthologues from other organisms. The three-helical bundle of the Pex14(N) domain comprises two hydrophobic cavities for recognition of two aromatic side chains, presented either by a classical WxxxF/Ymotif (Pex5) or by an F/YFxxxF sequence (Pex19), which we identified here by our structural and mutational analysis. Recognition of these peptides involves a combination of hydrophobic and electrostatic interactions, as shown by the analysis of a series of interface mutants (Figures 5 and 6). The Pex5–Pex14(N) interaction appears further stabilised by a salt bridge involving the conserved Lys56 in Pex14. A corresponding salt bridge is not observed in the structure of the Pex14(N)–Pex19 complex. However, the enhanced binding affinity for Pex19 Q72E or Q72D mutants (Figure 5) suggests that a corresponding interaction might be possible. The lack of this salt bridge in the wild-type Pex19 motif may contribute to the reduced binding affinity of the Pex19 peptide compared with the Pex5 motifs.

A surprising finding of our study is that Pex14(N) recognises the two helical ligands in opposite orientations. In this respect, it is interesting to note that site mapping of fungal Pex5 revealed that the Pex14(N) binding region contains an inverse WxxxF/Ymotif (Williams *et al*, 2005; Kerssen *et al*, 2006) and the *Saccharomyces cerevisiae* Pex5 sequence FQEVW resembles the human Pex19 core binding motif FQELF. It is possible that these sequences bind in an inverted orientation to Pex14(N) in these organisms. In preliminary experiments, we have confirmed that the *S. cerevisiae* Pex5 FQEVW motif binds to *S. cerevisiae* Pex14 (not shown), albeit the orientation of the peptide remains to be investigated experimentally. The ability of binding helical peptides with opposite directionality is unusual but has been observed before for few other interactions involving ligands of calmodulin (Osawa *et al*, 1999; Hoeflich and Ikura, 2002), SH3 domains (Feng *et al*, 1994; Lim *et al*, 1994; Kuriyan and Cowburn, 1997) and the Sin3 corepressor PAH2 domain (Swanson *et al*, 2004).

The Pex14(N)–Pex5 complex reveals the structural basis for an interaction that is critical for docking of the Pex5 import receptor to the peroxisomal membrane. The importance of the two aromatic residues and the consensus binding motifs identified by our mutational analysis are consistent with the reported interaction of Pex14 to other WxxxF/Y motifs in the N-terminus of Pex5 (Saidowsky *et al*, 2001) and the potential to form higher order Pex14–Pex5 complexes (Gouveia *et al*, 2000) by binding of multiple Pex14 proteins to the different WxxxF/Y motifs. Our *in vivo* experiments and *in vitro* binding studies of Pex14(N) mutants with Pex5 and Pex19 ligand motifs show a correlation between ligand-binding and peroxisomal localisation of Pex14. The mutational analysis of residues in the Pex14(N) ligand-binding surface shows that the N-terminal domain fulfils an important function in the topogenesis of Pex14. This is noteworthy because a canonical mPTS, consisting of a transmembrane domain and a positively charged amphipathic helix in the cargo, is not identifiable in Pex14 (Rottensteiner *et al*, 2004). Our data, thus, suggest that the Pex14 N-terminal domain might contribute to a composite mPTS in Pex14.

Previous studies have shown that Pex14 is mislocalised to mitochondria in Pex13 defective cells, and that the Pex14 N-terminus interacts with the SH3 domain of Pex13 *in vitro* (Fransen *et al*, 2004; Itoh and Fujiki, 2006). The mutational analysis in GST pull-down experiments by Fransen *et al* showed a reduced binding of full-length Pex14 mutants (F35S, L36R, F52S, K56E and L58R) to Pex13. Moreover, the K56E mutation was found by Fransen *et al* to impair binding of full-length Pex14 to Pex13 but not to Pex5 or Pex19. However, our structural analysis revealed that all these residues are located at the common binding surface of Pex14 for both Pex5 and Pex19 peptides (Supplementary Figure 6C), and in our experiments, the K56E mutation in Pex14(N) affects both the Pex5 and the Pex19 interaction (Figure 6A). Moreover, despite the presence of a potential SH3 binding PxxP motif in Pex14 (residues 24–27), we could not detect binding of Pex14(N) to the human Pex13 SH3 domain in NMR titrations (Supplementary Figure 6).

Taken together, the data suggest that (i) additional regions of Pex14, Pex19 and Pex13 may contribute to the binding of the full-length proteins and (ii) interactions between these proteins induce structural changes that modulate the binding affinities. For example, a structural change could expose a PxxP motif in the N-terminus of Pex14, which then could bind to the Pex13 SH3 domain. In addition, data from Fujiki and coworkers suggest that oligomerisation, possibly dimerisation of Pex14 is required for the interaction with Pex13 (Itoh and Fujiki, 2006). Pex14 targeting may thus also involve additional, so far unidentified regions in Pex14, Pex13 and Pex19, thus explaining the different experimental

 

observations when comparing full-length and minimal interaction domains.

Another mechanistic implication of our data results from the observation that Pex19 and Pex5 directly compete for binding with Pex14(N) *in vitro*. The binding affinity of Pex14(N) to Pex5 is about 130-fold stronger than to Pex19. Moreover, Pex5 possesses seven of the high-affinity WxxxF/Y ligands. If these binding features are maintained in the full-length proteins, Pex5 would quantitatively replace Pex19 bound to Pex14 wherever these proteins colocalise *in vivo*.

In summary, we present a structural and biochemical characterisation of the conserved N-terminal domain of Pex14 and its molecular recognition of Pex5 and Pex19 ligands, two central proteins in peroxisomal biogenesis. We show that Pex5 and Pex19 compete for binding to a common site in Pex14 *in vitro*. The discovery of a new pseudo-symmetrical F/YFxxxF interaction motif in Pex19 indicates a broader spectrum of possible Pex14 binding partners. Thus, our structural data reveal details about the molecular prerequisites for Pex14 ligands and provides the framework for the prediction of further possible interaction partners.

## Materials and methods

### *Protein expression and isotope labelling*

Human Pex14(N) (residues 16–80) and Pex13(SH3) (residues 257–344) were expressed from a pETM-11 vector (G. Stier, EMBL Heidelberg) in *E. coli* BL21(DE3). A Pex14 expression construct with an additional C-terminal tryptophan (Pex14 16–80W) facilitated detection during purification but did not alter the Pex5 or Pex19 interaction (Supplementary Figure 2C and D). Expression incorporated an N-terminal hexahistidine ($His_6$) fusion followed by a tobacco etch virus (TEV) proteolytical cleavage site. Pex14(N) (16–78) A32W, V41W, F52W and (16–80W) T31A, N38A, V41A, K34A, R49E, F52A, K56E, K56A mutants were created through Stratagene QuikChange Site-Directed Mutagenesis Kit according to the manufacture's manual. Cultures were grown in LB medium with 1% (w/v) glucose and induced mid-log-phase with 0.5 mM IPTG overnight at 25°C. Isotopically labelled ($^{13}C$ and/or $^{15}N$) Pex14 was prepared by growing bacteria in minimal medium supplemented with [U-$^{13}C$] glucose and/or $^{15}NH_4Cl$. Cell pellets were resuspended, lysed by sonication in the presence of protease inhibitors, and the lysate was cleared by centrifugation. The lysate was purified by affinity Ni-NTA agarose (QIAgen). After an overnight incubation with $His_6$ fusioned TEV protease (1 mg protease/25 mg protein), a second Ni-NTA agarose column removed uncleaved product, the $His_6$ fusion and the protease. Pex5 and Pex19 peptides for NMR and calorimetry were prepared by solid-phase synthesis by Dr Martin Jung and Ramona Gölzer (University of Saarland, Germany).

### *NMR spectroscopy and structure calculation*

Proteins/complexes were exchanged into 50 mM sodium phosphate with 100 mM NaCl (pH 6.5) by gel filtration. Samples were measured at concentrations of 0.2–1.0 mM in $H_2O$ or $^2H_2O$. All NMR spectra were acquired at 303 K on a Bruker DRX500 or Bruker DRX600 spectrometer with cryogenic probe, except from a 2D $^1H$-NOESY acquired on a Bruker DRX900 spectrometer with triple resonance probe. Backbone and side-chain chemical shifts of Pex14(N) were obtained using standard triple resonance experiments. Assignments of the peptide ligands and intermolecular distance restraints were obtained from X-filtered 2D and 3D NOE experiments (Sattler *et al*, 1999). Chemical shift perturbations ($\Delta\delta = [(\Delta\delta^1H)^2 + (1/5\ \Delta\delta^{15}N)^2]^{1/2}$, in parts per million) were monitored in two-dimensional $^1H$,$^{15}N$-HSQC experiments. $H^N$-N and N-C' residual dipolar couplings were measured for the Pex14–Pex5 complex in a Pf1 phage liquid crystalline medium (Rückert and Otting, 2000). The experimentally determined distance, dihedral and dipolar coupling restraints were applied in a simulated annealing protocol using ARIA1.2 (Linge *et al*, 2003a) The final ensemble of NMR structures was refined in a shell of water molecules (Linge *et al*, 2003b). For the Pex14–Pex5 and Pex14–Pex19 complexes, 90.0%/9.0% and 91.8%/6.7% of the backbone dihedral angles in the final NMR ensemble are in the most favoured and allowed regions of the Ramachandran plot, respectively, analysed with PROCHECK (Laskowski *et al*, 1993). For further details see Supplementary data.

### *ITC*

Proteins and ligands were co-dialysed against 50 mM potassium phosphate buffer with 100 mM NaCl at pH 6.6. Dialysates were degassed and the concentration measured by $A_{280\,nm}$. ITC measurements were conducted on a MicroCal VP-ITC using Pex14(N) at 25–57 μM as a sample and Pex5 or Pex19 peptides at 500–700 μM as the titration ligand. Per experiment 18 subsequent injections of 10–12 μl were separated by time intervals of 300 s to allow adjustment of equilibration. All ITC experiments were conducted at a stirring speed of 300 rpm at 297 K using injection protocols found to saturate Pex14(N) with ligand. Ligand heats of dilution were subtracted. Data were fitted using MicroCal™ Origin™ 5.0 (www.microcal.com) assuming a 1:1 complex stoichiometry.

### *Peptide spot overlay assays*

Peptides comprising 15 amino acids, representing Pex5(113–127) and Pex19(66–80) or variations of both were directly synthesised on a cellulose membrane as described previously (Saidowsky *et al*, 2001). Membranes were blocked with 3% BSA in TBS (10 mM Tris–HCl pH 7.4, 150 mM NaCl) and incubated overnight at 4°C with 1 μM or 45 nM $His_6$-tagged Pex14(N) wild-type or mutant protein in TBS. The membranes were blocked again with TBS + 3% BSA and for immunochemical detection of His-tagged Pex14 on the membrane anti-Pex14 antibodies (Will *et al*, 1999) or monoclonal anti-$His_6$ antibodies in TBS + 3% BSA, horseradish peroxidase-coupled secondary antibodies in TBS + 10% milk powder and ECL Western Blotting Detection Reagent (GE Healthcare Amersham ECL Western Blotting Detection Reagent) were used. Between these steps, the membranes were thoroughly washed with TBS-TT (20 mM Tris–HCl pH 7.5, 0.5M NaCl, 0.05% (v/v) Tween20, 0.2% (v/v) Triton X-100), and at the end of each washing step, the membranes were washed with TBS only.

### *Fluorescence microscopy*

Human fibroblast cells were cultured as described previously (Stanley *et al*, 2006). The primary Pex14-deficient cell line K-01 (Shimozawa *et al*, 2004) was first immortalised by transfecting SV-40 large T antigen. The resulting cell line K-01 T was double-transfected with plasmids expressing full-length Pex14 variants alone or together with EGFP-SCP2—expressing plasmid (Stanley *et al*, 2006), referred to as GFP-PTS1, using Amaxa Nucleofector-Kit. Forty-eight hours after transfection, cells were subjected to fluorescence and immunofluorescence microscopy using antibodies against *Hs*Pex14 (Will *et al*, 1999) and against the mitochondrial marker protein TRAP 1 (ABR, Affinity Bioreagents). The secondary antibodies used for Pex14-labelling were anti-rabbit IgGs conjugated with a fluorophor, either Alexa Fluor 488 or Alexa Fluor 594 (Molecular Probes). The preparation of cells as well as the recording and processing of micrographs was carried out as described previously (Will *et al*, 1999).

### *Accession codes*

The atomic coordinates of the Pex14–Pex5 and the Pex14–Pex19 complexes have been deposited in the Protein Data Bank under accession code 2W84 and 2W85, respectively.

### *Supplementary data*

Supplementary data are available at *The EMBO Journal* Online (http://www.embojournal.org).

## Acknowledgements

We thank Dr Martin Jung and Ramona Gölzer (University of Saarland, Germany) for immobilised peptide synthesis and Gunter Stier (EMBL) for protein expression vectors. This work was supported by the Deutsche Forschungsgemeinschaft (SFB 594 and Sa823/5 to MS; Schl584/1-1 to WS), and the grants 3D Repertoire (LSHG-CT-2005-512028 to MS and MW) and LSHG-CT-2004-512018 (to RE) from the European Commission.

## References

Albertini M, Rehling P, Erdmann R, Girzalsky W, Kiel JA, Veenhuis M, Kunau WH (1997) Pex14p, a peroxisomal membrane protein binding both receptors of the two PTS-dependent import pathways. *Cell* **89:** 83–92

Choe J, Moyersoen J, Roach C, Carter TL, Fan E, Michels PA, Hol WG (2003) Analysis of the sequence motifs responsible for the interactions of peroxins 14 and 5, which are involved in glycosome biogenesis in Trypanosoma brucei. *Biochemistry* **42:** 10915–10922

Erdmann R, Schliebs W (2005) Peroxisomal matrix protein import: the transient pore model. *Nat Rev Mol Cell Biol* **6:** 738–742

Feng S, Chen JK, Yu H, Simon JA, Schreiber SL (1994) Two binding orientations for peptides to the Src SH3 domain: development of a general model for SH3-ligand interactions. *Science* **266:** 1241–1247

Fransen M, Brees C, Ghys K, Amery L, Mannaerts GP, Ladant D, Van Veldhoven PP (2002) Analysis of mammalian peroxin interactions using a non-transcription-based bacterial two-hybrid assay. *Mol Cell Proteomics* **1:** 243–252

Fransen M, Vastiau I, Brees C, Brys V, Mannaerts GP, Van Veldhoven PP (2004) Potential role for Pex19p in assembly of PTS-receptor docking complexes. *J Biol Chem* **279:** 12615–12624

Fransen M, Vastiau I, Brees C, Brys V, Mannaerts GP, Van Veldhoven PP (2005) Analysis of human Pex19p's domain structure by pentapeptide scanning mutagenesis. *J Mol Biol* **346:** 1275–1286

Gouveia AM, Reguenga C, Oliveira ME, Sa-Miranda C, Azevedo JE (2000) Characterization of peroxisomal Pex5p from rat liver. Pex5p in the Pex5p-Pex14p membrane complex is a transmembrane protein. *J Biol Chem* **275:** 32444–32451

Halbach A, Landgraf C, Lorenzen S, Rosenkranz K, Volkmer-Engert R, Erdmann R, Rottensteiner H (2006) Targeting of the tail-anchored peroxisomal membrane proteins PEX26 and PEX15 occurs through C-terminal PEX19-binding sites. *J Cell Sci* **119:** 2508–2517

Halbach A, Lorenzen S, Landgraf C, Volkmer-Engert R, Erdmann R, Rottensteiner H (2005) Function of the PEX19-binding site of human adrenoleukodystrophy protein as targeting motif in man and yeast. PMP targeting is evolutionarily conserved. *J Biol Chem* **280:** 21176–21182

Hoeflich KP, Ikura M (2002) Calmodulin in action: diversity in target recognition and activation mechanisms. *Cell* **108:** 739–742

Itoh R, Fujiki Y (2006) Functional domains and dynamic assembly of the peroxin Pex14p, the entry site of matrix proteins. *J Biol Chem* **281:** 10196–10205

Kerssen D, Hambruch E, Klaas W, Platta HW, de Kruijff B, Erdmann R, Kunau WH, Schliebs W (2006) Membrane association of the cycling peroxisome import receptor Pex5p. *J Biol Chem* **281:** 27003–27015

Kuriyan J, Cowburn D (1997) Modular peptide recognition domains in eukaryotic signaling. *Annu Rev Biophys Biomol Struct* **26:** 259–288

Laskowski R, MacArthur M, Thormton J (1993) PROCHECK: a program to check the stereochemical quality of protein structures. *J Appl Cryst* **26:** 283–291

Lim WA, Richards FM, Fox RO (1994) Structural determinants of peptide-binding orientation and of sequence specificity in SH3 domains. *Nature* **372:** 375–379

Linge JP, Habeck M, Rieping W, Nilges M (2003a) ARIA: automated NOE assignment and NMR structure calculation. *Bioinformatics* **19:** 315–316

Linge JP, Williams MA, Spronk CA, Bonvin AM, Nilges M (2003b) Refinement of protein structures in explicit solvent. *Proteins* **50:** 496–506

Osawa M, Tokumitsu H, Swindells MB, Kurihara H, Orita M, Shibanuma T, Furuya T, Ikura M (1999) A novel target recognition revealed by calmodulin in complex with Ca2 + -calmodulin-dependent kinase kinase. *Nat Struct Biol* **6:** 819–824

Otera H, Setoguchi K, Hamasaki M, Kumashiro T, Shimizu N, Fujiki Y (2002) Peroxisomal targeting signal receptor Pex5p interacts with cargoes and import machinery components in a spatiotemporally differentiated manner: conserved Pex5p WXXXF/Y motifs are critical for matrix protein import. *Mol Cell Biol* **22:** 1639–1655

Rottensteiner H, Kramer A, Lorenzen S, Stein K, Landgraf C, Volkmer-Engert R, Erdmann R (2004) Peroxisomal membrane proteins contain common Pex19p-binding sites that are an integral part of their targeting signals. *Mol Biol Cell* **15:** 3406–3417

Rückert M, Otting G (2000) Alignment of biological macromolecules in novel nonionic liquid crystalline media for NMR experiments. *J Am Chem Soc* **122:** 7793–7797

Sacksteder KA, Jones JM, South ST, Li X, Liu Y, Gould SJ (2000) PEX19 binds multiple peroxisomal membrane proteins, is predominantly cytoplasmic, and is required for peroxisome membrane synthesis. *J Cell Biol* **148:** 931–944

Saidowsky J, Dodt G, Kirchberg K, Wegner A, Nastainczyk W, Kunau WH, Schliebs W (2001) The di-aromatic pentapeptide repeats of the human peroxisome import receptor PEX5 are separate high affinity binding sites for the peroxisomal membrane protein PEX14. *J Biol Chem* **276:** 34524–34529

Sattler M, Schleucher J, Griesinger C (1999) Heteronuclear multidimensional NMR experiments for the structure determination of proteins in solution employing pulsed field gradients. *Prog NMR Spectrosc* **34:** 93–158

Saveria T, Halbach A, Erdmann R, Volkmer-Engert R, Landgraf C, Rottensteiner H, Parsons M (2007) Conservation of PEX19-binding motifs required for protein targeting to mammalian peroxisomal and trypanosome glycosomal membranes. *Eukaryot Cell* **6:** 1439–1449

Shimizu N, Itoh R, Hirono Y, Otera H, Ghaedi K, Tateishi K, Tamura S, Okumoto K, Harano T, Mukai S, Fujiki Y (1999) The peroxin Pex14p. cDNA cloning by functional complementation on a Chinese hamster ovary cell mutant, characterization, and functional analysis. *J Biol Chem* **274:** 12593–12604

Shimozawa N, Tsukamoto T, Nagase T, Takemoto Y, Koyama N, Suzuki Y, Komori M, Osumi T, Jeannette G, Wanders RJ, Kondo N (2004) Identification of a new complementation group of the peroxisome biogenesis disorders and PEX14 as the mutated gene. *Hum Mutat* **23:** 552–558

Stanley WA, Filipp FV, Kursula P, Schuller N, Erdmann R, Schliebs W, Sattler M, Wilmanns M (2006) Recognition of a functional peroxisome type 1 target by the dynamic import receptor pex5p. *Mol Cell* **24:** 653–663

Swanson KA, Knoepfler PS, Huang K, Kang RS, Cowley SM, Laherty CD, Eisenman RN, Radhakrishnan I (2004) HBP1 and Mad1 repressors bind the Sin3 corepressor PAH2 domain with opposite helical orientations. *Nat Struct Mol Biol* **11:** 738–746

Wanders RJ, Waterham HR (2006) Biochemistry of mammalian peroxisomes revisited. *Annu Rev Biochem* **75:** 295–332

Will GK, Soukupova M, Hong X, Erdmann KS, Kiel JA, Dodt G, Kunau WH, Erdmann R (1999) Identification and characterization of the human orthologue of yeast Pex14p. *Mol Cell Biol* **19:** 2265–2277

Williams C, van den Berg M, Distel B (2005) Saccharomyces cerevisiae Pex14p contains two independent Pex5p binding sites, which are both essential for PTS1 protein import. *FEBS Lett* **579:** 3416–3420

 